2022

Power Management in Hybrid ANFIS PID Based AC−DC Microgrids with EHO Based Cost Optimized Droop Control Strategy

T. Narasimha Prasad

Research paper

Power management in hybrid ANFIS PID based AC–DC microgrids with EHO based cost optimized droop control strategy

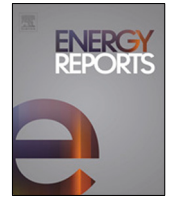T. Narasimha Prasad [a], S. Devakirubakaran [b], S. Muthubalaji [c], S. Srinivasan [d], Karthikeyan B. [e], Palanisamy R. [f], Mohit Bajaj [g], Hossam M. Zawbaa [h,i,j,*], Salah Kamel [k]

[a] St Ann's College of Engineering and Technology, Andra Pradesh, India
[b] QIS College of Engineering and Technology, Andra Pradesh, India
[c] Department of EEE, CMR College of Engineering & Technology, Telangana, India
[d] Department of Electrical & Electronics, CMR College of Engineering & Technology, Telangana, India
[e] Department of EEE, K. Ramakrishnan College of Technology, India
[f] Department of EEE, SRM Institute of Science and Technology, India
[g] Department of Electrical Engineering, Graphic Era (Deemed to be University), Dehradun 248002, India
[h] Faculty of Computers and Artificial Intelligence, Beni-Suef University, Beni-Suef, Egypt
[i] Technological University Dublin, Dublin, Ireland
[j] Applied Science Research Center, Applied Science Private University, Jordan
[k] Electrical Engineering Department, Faculty of Engineering, Aswan University, 81542 Aswan, Egypt

ABSTRACT

One of the most critical operations aspects is power management strategies for hybrid AC/DC microgrids. This work presented power management in hybrid AC–DC microgrids with a droop control strategy. At first, photovoltaic, Wind, and battery are used as the power sources, which supply the power with uncertainties. The AC and DC microgrids are controlled by an Adaptive neuro-fuzzy inference system (ANFIS) controller and Proportional Integral Derivative (PID) controller. Simultaneously we calculate the running cost for photovoltaic, Wind, and Battery. Moreover, an optimizer based on the elephant herding optimization algorithm is formulated to reduce the cost price. This method utilizes two stages like clan updating operator and separating operator. This cost value is used to calculate the Droop Coefficients in Droop Control Strategy. The autonomous droop control strategy is utilized in the interlinking converter to share the load between AC and DC. This proposed concept is implemented in the MATLAB tool, and the performance is taken in terms of voltage, power, and current for PV and wind, DC link voltage and load current. The bidirectional ac/dc interlinking converter power flow was subsequently changed from 2.2k W to −2k W. The effectiveness of the power dispatch mode under uniform control has been verified.

1. Introduction

Microgrid (MG) can be characterized as a lot of distribution generators (DGs) and interrelated loads with particular electric limits. Due to its various points of advantages relevant to power supply, MG has had major consideration in recent days (Wang et al., 2021). MGs work in islanded mode or grid connected mode. The ability of MG to work in an islanded mode is a feature

execution (Naderi et al., 2020). The execution of MG in these two modes depends on its assembly with the main service grid. From the main grid, if MG is separated, then it can work in islanded method, or else it will work in a grid connected mode (Naidu and Meikandasivam, 2020). As a result, MG is constantly accessible in any condition, whether there is a defect in the main grid or not. Many research processes have already been done depending on MG's execution enhancement. In AC MGs (Shravan and Vyjayanthi, 2020), the loads and DGs are linked with the bus AC. DC units are consolidated in the system by utilizing the DC–AC converters, and DC loads are provided using inverters. DC load requires DC supply for operation, and AC loads need AC supply (Islam et al., 2020). Because of an AC MG, the DC loads are provided by utilizing AC–DC inverters. In any case, there will be a proficiency decrement if the power system of AC supplies the DC loads. DC based MG (Gupta et al., 2020; Hesaroor and Das,

* Correspondence to: Technological University Dublin, Park House, 191 N Circular Rd, Cabra East, Grangegorman, Dublin, D07 EWV4, Ireland.
E-mail addresses: narasimhaiete@gmail.com (T.N. Prasad), kirubathas@gmail.com (S. Devakirubakaran), muthusa15@gmail.com (S. Muthubalaji), s.srinivasan2906@gmail.com (S. Srinivasan), karthikeyanb.eee@krct.ac.in (Karthikeyan B.), krspalani@gmail.com (Palanisamy R.), thebestbajaj@gmail.com (M. Bajaj), hossam.zawbaa@gmail.com, hossam.elsayed@tudublin.ie (H.M. Zawbaa), skamel@aswu.edu.eg (S. Kamel).

Nomenclature

I_{PV}	Photovoltaic cell
I_{PH}	Photovoltaic current
I_P	Light generated PV current
I_D	Polarization of the p–n junction current
I_{PH}^{STC}	Standard condition light-generated PV current
I_O	Diode current
K_i	Temperature current constant
IR_{sh}	Current in the resistor
G	Actual Irradiance level
G_{STC}	STC condition irradiance of PV
T_j	Cell temperature
V_{OC}	Open circuit current
V_{PV}	Photovoltaic voltage
V_{INmin}	Minimum input voltage
V_{out}	Desired output voltage
η	Efficiency of the converter
D	Duty cycle
L	Selected inducted value
f_s	Minimum switching frequency of converter
S	Area traversed by rotor blades
ρ	Air density
R	Rotor blade radius
λ	Tip speed ratio
I_{bat}	Discharge current
V_{cell}	Open circuit voltage of single cell
R_{bat}	Equivalent series resistance of the battery cell
P_{bat}	Total demand power from battery
n_{bat}	Total number of battery cells
K_b	Rated capacity expressed in Amps-hour
$SOC(t)$	State of charge of battery in time
SOC_{int}	Initial state of charge
R_S	Reverse saturation current
I_S	Series resistance
V_t	Thermal voltage
α	Ideality factor
T	Junction temperature
Q	Charge of electron
K	Boltzmann's constant
C_P	Coefficient of power
ω	Rotor angular speed
$k\&c$	Shape and scalar factor of wind turbine
v	Current wind speed
δ	Sum of solar irradiance
$\omega\&\psi$	Beta PDF parameter
K_P	Proportional gain
K_i	Integral gain
$V, V_{max}, K_{dc}\&P_{dc}$	Dc link voltage, no load dc link voltage, droop gain and converter output power
$P_{DC,n}$	Converter rated power
f_{ac}	Reference frequency
f_{max}	No load maximum frequency condition
P_{ac}	Inverter output power
K_{ac}	Droop gain slope
$P_{ac,n}$	Inverter rated power
$V_{I,N}$	Dc terminal voltage of interlinking converter
P_d	Demand power
$C_{G,i}(G_i)$	Total active power generation cost of ith generator
$C_{G,e,i}(G_i)$	Emission penalty for concerned generator
$C_{G,m,i}(G_i)$	Maintenance cost
$x_{new,ki,j}$	Modern position of j in clan i
$x_{ki,j}$	Older position
$x_{best,ki,j}$	Finest solution of clan k_i
$\alpha \in [0, 1]$	Algorithms parameter
$X_{max}\&x_{min}$	Upper and lower bound
$n_{q,i,c}$	Reactive power droop coefficient
$m_{p,i,c}$	Active power droop coefficient

2020) is a framework with rectifiers and inverters for AC and DC, respectively.

In this method, AC sources like ordinary AC loads, diesel generators and wind turbine generators (WTGs) are associated with the AC network; also, the DC sources like DC loads, fuel generators, and PV generators are associated with the DC grid. Most of the modern research papers depend on AC and DC, hybrid MGs, in which AC MGs have the most number when contrasted with the DC grid. Single-stage high-frequency AC MG is planned in Kumar et al. (2020) for energy management in AC microgrids. A familiar hierarchical multi-level device for AC and DC microgrids is suggested in Zhang et al. (2020). PSO based MG controlling with diminished expense (Faisal et al., 2020; Grisales-Noreña et al., 2020), Berkeley Lab's dispersed energy assets client acceptance model (Narang et al., 2021), ideal interest technique for a wind electric generator (WEG) (Reyes et al., 2020), a GA based energy management (Fu et al., 2020) in which the controlling can confirm the load appeal during 24 h working with most minimal power rate, are suggested for the energy management in MGs. The performance of energy management in MGs is portrayed in Jafari et al. (2020). Based on the non-linear control method, the distributed energy storage system was designed (Toghani Holari et al., 2020) in grid connected operation for hybrid microgrid power management. A power management algorithm based multi-functional three phase grid connected PV for conservative power was designed by Oruganti et al. (2020). Power management and power quality enhancement for PV and battery storage system was designed by Mousazadeh Mousavi et al. (2018). Energy management system (EMS) for the DC MGs that causing a decrease in contamination (Hannan et al., 2020), EMS dependent on fuzzy logic (Dewangan et al., 2021) are proposed to enhance power distribution among energy units on account of a DC MG. Since the regular matrix utilizes AC, in a few applications, we require DC supply. So transformation is needed among AC and DC. However, because of the existence of transformation, misfortunes number of converters ought to be decreased. For this situation, the DC system should create to moderate this issue. Such systems give various preferences like accuracy enhancement and small spaces of segments (Han et al., 2020; Sridhar and Kowsalya, 2021). A Hybrid AC–DC MG energy management system is created in Peña-Aguirre et al. (2020), in which the RES and energy storage systems (ESS) are integrated. The proposed method can solve the presence of uncertainties

like photovoltaic output power, wind turbine, active and reactive power, cost, and load demand.

The contribution of the work states that,

- To generate the power from PV and wind, the battery is used to store the power for power management.
- To control AC and DC microgrids by Adaptive neuro-fuzzy inference system controller and Proportional Integral Derivative (PID) controller.
- To calculate the running cost for PV, wind, and battery by Elephant Herding Optimization (EHO) algorithm.
- The proposed work is implemented through the MATLAB platform, and the performances are analyzed graphically to show the effectiveness of the proposed work.

The overall methodology for planned research work is organized as follows. Section 2 gives some relevant literature survey related to our proposed work. Section 3 gives the proposed methodology flow, including mathematical modeling of PV, wind, storage, DC-subgrid, AC-subgrid, interlinking converter, cost reduction by EHO, and droop control strategy. Section 4 gives the graphical analysis of performance metrics for several parameters, and Section 5 shows the experimental setup. The conclusion about the proposed work is given in Section 6.

2. Literature survey

A GPS based decentralized controlling method was presented by Esfahani and Savaghebi (2021) for hybrid AC/DC microgrids. In AC/DC subgrids, V–I droop characteristics were utilized for distributed energy resources (DERs). The DER output voltage was adjusted as a piecewise linear function. To get the global power sharing between AC/DC DERs, a droop control scheme was used. The AC bus voltage deviation was changed by interlink converter as a function of DC bus voltage deviation. A decentralized generation storage subgrid coordination control was proposed by Lv et al. (2020) to assure the state of charge (SOC) protection and power limitations for power management. A modified droop scheme is adapted in the battery energy storage control strategy to deliver output power and SOC signal. In a bidirectional power converter, a fuzzy logic controller was adopted to prevent battery energy storage overuses. Moreover, a modified perturb and observe method was applied in PV systems. In hybrid AC/DC microgrids, the parallel interlinking converters (ICs) operations were addressed by Alsiraji and El-Shatshat (2021). The parallel ICs were addressed by a unified mitigation technique. At first, the non-linearity system influence on circulating current among parallel interlinking converters was examined. After that, because of antiparallel diodes, the ICs should induce voltage harmonics. Finally, the abnormal operating conditions were discussed. An enhanced virtual synchronous machine with a dual droop controller was designed to improve the ICs operations.

A novel distributed secondary control method was presented by Espina et al. (2020) for hybrid AC/DC. The frequency and AC/DC voltage magnitude were regulated simultaneously using the controllers, including the interlinking converter by distributed consensus method in the control method. The secondary control restoration and power sharing accuracy were improved on both AC/DC sides. A centralized non-linear controller was investigated by Armghan et al. (2020) for a hybrid AC/DC microgrid, which depends on fast integral and integral terminal sliding mode. Initially, AC/DC microgrid mathematical model was established. After that, during grid connected and islanding mode, the controller was designed to ensure the constant AC/DC bus voltage. The controller was given frequency support to the grid during the grid connected mode.

Based on the technical modeling of several typical components, a genetic algorithm (GA) design method was used by Mayer et al. (2020) for household scale systems. One of the control methods was internal model control (IMC) for controller design based on a mathematical model. Zeng et al. (2020) adopted the IMC with PSO algorithm, which includes PID proportional integral derivative (PID) controllers for controlling the core power. Nowadays, the globe is increasingly oriented toward the use of renewable energy sources to reduce the consumption of traditional energy sources, particularly fuel energy. Furthermore, the utilization of renewable energy sources reduces the environmental effect of conventional energy. For all of these reasons, researchers are presently concentrating their efforts on studies that apply and create ways to improve and boost the efficiency of existing renewable energy sources. Hybrid systems are one of the proposed techniques. These systems may be used in both the household and industrial sectors. Hybrid systems, on the other hand, can be used in renewable energy, wind energy, fuel cell, desalination, heating, ventilation, and air conditioning, engines, electric vehicles, heat pumps, redrying, PV cells, engines, solar cells, and many other systems. A brief current assessment of the kinds and uses of hybrid renewable energy systems and hybrid recovery energy systems used in the industrial and residential sectors. In addition, the environmental effect, cost, and efficiency will be presented and addressed. The various hybrid energy systems are discussed, and a critical analysis is carried out (Farhat et al., 2022). The low-voltage AC/DC hybrid power distribution system is quickly becoming an essential component of the future power grid. Because of the high proportion of power electronics and renewable energy supplies, the system is subject to several uncertainties. Based on reachability analysis, a dynamic performance analysis approach of a low-voltage AC/DC hybrid power distribution system under numerous uncertainties, which illustrates the time-varying trajectory and boundary of the system state variables, was discussed. The usual structure of a low-voltage AC/DC hybrid distribution system is first examined. The associated differential–algebraic equations (DAEs) are defined. The fundamental theoretical approach of reachability analysis is then given. The approach is then expanded to include low-voltage AC/DC hybrid power distribution systems. Finally, the MATLAB/Simulink platform is used to evaluate situations such as bus load volatility and renewable energy supplies. This dynamic performance analysis approach is validated by a comparative study of reachability analysis and time-domain simulation. With an increasing number of uncertainties, the dynamic performance study would give technical support for a low-voltage AC/DC hybrid power distribution system (Ding et al., 2022). An optimized designing parameters for the hybrid switch have been discussed and valuable considerations for establishing the hybrid connection has provided (Qin et al., 2022). The difficulties faced by the low wind speed turbines and high wind speed turbines are discussed and a new kind of composite and PLA material based wind turbines are fabricated with enhanced performances (Aljafari et al., 2022). The power affecting factors in the solar photovoltaic system has been discussed and the required solutions and recommendations are provided for enhancing the power conversion efficiency of the solar photovoltaic systems (Cherukuri et al., 2021). By reducing the power affecting factors in renewable energy systems, the voltage and current fluctuations in hybrid systems can be overcome through the necessary provisions.

3. Proposed method

Initially, here we are choosing two PV, two Wind, and two batteries for power management, generating the power from PV and wind with some uncertainties. Then uncertainties are
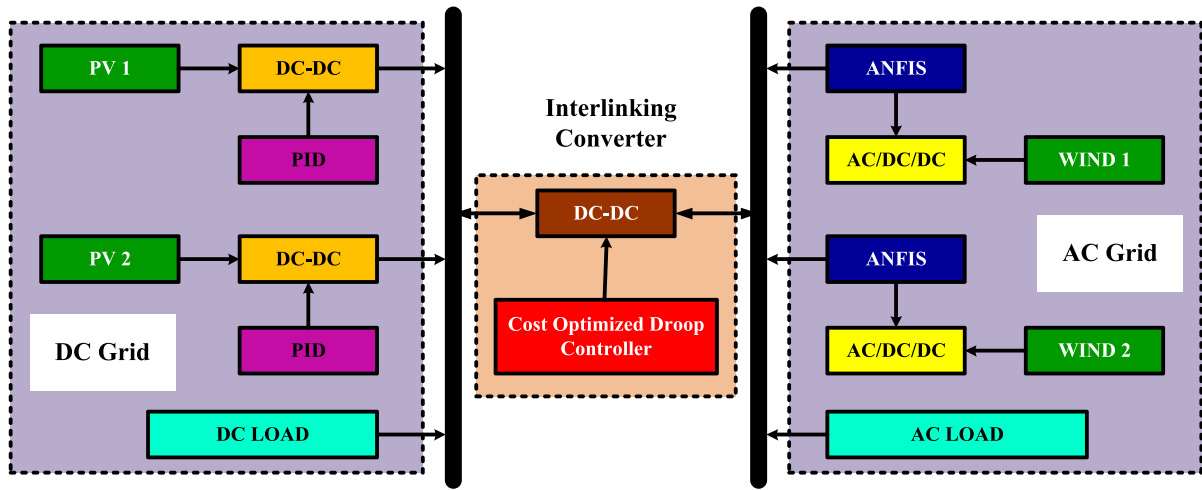
Fig. 1. Proposed diagram.

estimated from the generation systems. The DC grid is controlled by the PID controller, and the AC grid is controlled by the ANFIS controller. Simultaneously we calculate the running cost for PV, Wind, and Battery. This total cost is minimized by using Elephant Herding Optimization (EHO) Algorithm. This cost value is used to calculate the Droop Coefficients in Droop Control Strategy. Then the autonomous interlinking droop control strategy is utilized to interlinking both AC and DC. Load sharing is performed between the hybrid AC and DC sub-grid. Fig. 1 shows the working procedure for this work. Fig. 2 shows the flow chart of the entire proposed process.

3.1. Mathematical modeling of PV system

More than one solar panels in PV that mingled inverter and other hardware such as mechanical and electrical, which utilize energy to produce electricity from the sun.

PV current (Roumila et al., 2017)
The PV module output current can be described in Eq. (1),

$$I_{PV} = I_{PH} - I_D - I_P \tag{1}$$

where light-generated PV current is denoted as I_P, it is expressed in Eq. (2),

$$I_{PH} = \left(I_{PH}^{STC} + K_i dt\right) \frac{G}{G^{STC}} \tag{2}$$

Here I_{PH}^{STC} and k_i are represent the standard condition light-generated PV current and temperature current constant, respectively. Actual irradiance and STC condition irradiance of PV is described as G and G^{STC}. Then the diode current is I_0 described in Eq. (3)

$$I_D = I_s \left(e^{\left(\frac{(V_{pv}+I_l R_s)}{aV_t}\right)} - 1\right) \tag{3}$$

where reverse saturation current and series resistance is indicated as R_s and I_s, respectively. The reverse saturation current and thermal voltage V_t is calculated by Eqs. (4) and (5),

$$I_s = \left(I_s^{STC} + K_i dt\right) \frac{G}{G^{STC}} \tag{4}$$

$$V_t = \frac{\alpha k T}{q} \tag{5}$$

Under STC conditions, reverse saturation current is denoted as I_s^{STC}, ideality factor is indicated as α, junction temperature (T), and
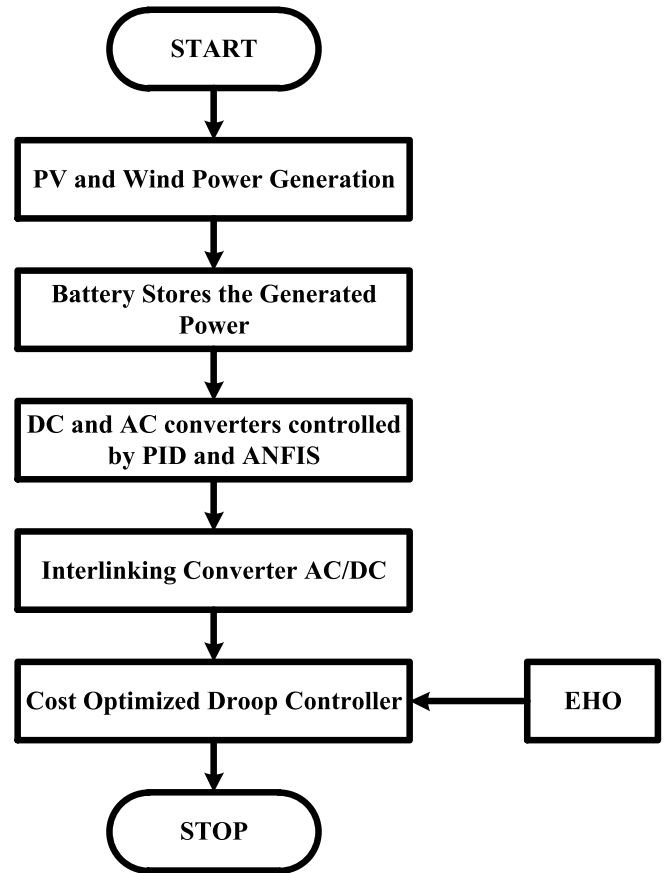

Fig. 2. Flow chart of entire proposed process.

electron charge q is $1.602 \times 10^{-19} C$. The Boltzmann's constant k is 1.3806×10^{-23}. Then shunt leakage current can be expressed as Eq. (6)

$$I_p = \frac{(V_{pv} + I_l R_s)}{R_P} \tag{6}$$

Here, V_{pv} is denoted as PV output voltage.

3.2. Mathematical modeling of wind energy systems

The Coefficient of Power (Manyonge et al., 2012),

$$C_P = \frac{2.P_{WIND}}{\lambda.S.V^3{}_{WIND}} \tag{7}$$

The wind turbine torque and output power will calculate by using the below equations,

Wind power

$$P_{WIND} = \frac{1}{2} C_p(\lambda).\rho.S.V^3{}_{WIND} \tag{8}$$

Tip speed Ratio

$$\lambda = \frac{\omega R}{V} \tag{9}$$

R is denoted as rotor blade radius, and rotor angular speed is ω rad/s.

Wind torque

$$t_{WIND} = t_{MEC} = \frac{1}{2} \frac{cp(\lambda).\rho.R.S.V^2{}_{wind}}{\lambda} \tag{10}$$

3.3. Mathematical modeling of storage modeling (Allaoua et al., 2017)

Battery voltage

$$V_{BAT} = V_{CELL}.n_{BAT} \tag{11}$$

Battery current

$$I_{BAT} = \frac{v_{CELL} - \sqrt{v^2{}_{CELL} - 4R_{BAT}\left(p_{reqBAT}/n_{BAT}\right)}}{2R_{BAT}} \tag{12}$$

State of charge (SOC)

$$soc(t) = soc_{INTt} - \int_o^t \frac{I_{BAT}(t)}{3600\,k_b}\,dt \tag{13}$$

Total output power

$$p_{BAT} = v_{BAT}.I_{BAT} \tag{14}$$

Uncertainties of wind and PV

The probability difference between the forecasted and real value is known as uncertainty. The uncertainties of wind and PV are modeled to solve probabilistic issues. The generation of wind power is greatly based on wind speed variation. To model the characteristics of wind speed, we utilized the Weibull probability density function (PDF). So the PDF can be expressed as below:

$$PDF(v) = \frac{k}{c}\left(\frac{v}{c}\right)^{k-1} \exp\left(-\left(\frac{v}{c}\right)^k\right)(v \succ 0) \tag{15}$$

where, k and c is represented as shape and scalar factor of a wind turbine. v is represented as current wind speed.

The ambient temperature, module characteristics, and solar irradiance are basically dependent on power generation from the PV module. To model the solar irradiances, the method of Beta PDF is the best duration function. The below expression is formulated by distribution:

$$PDF(\xi) = \begin{cases} \dfrac{\Gamma(\omega + \psi)}{\Gamma(\omega)\Gamma(\psi)} \times \xi^{\omega-1}(1 - \xi)^{\psi-1} \\ 0 \end{cases} \tag{16}$$
$$\text{for } 0 \le \xi \le 1, \omega \ge 0, \psi \ge 0$$

where δ is represented as the sum of solar irradiance in kW/m², ω and ψ is represented as beta PDF parameter.

3.4. DC sub-grid

The DC sub-grid is combined with three interconnected buses consisting of PV, battery, and dc load. The PV voltage can be controlled by using the PID controller. DC output voltage is regulated by the PID control scheme. This controller creates the closed-loop system; the proportional controller output has the error signal multiplied using a constant as the gain value. A steady state error between the variable and fixed signals produces an unstable system.

$$PID = K_P e + K_i \int edt + K_d \frac{d}{dt}(e) \tag{17}$$

The controller output depends upon the integral error signal. The plant model is taken in Nayak et al. (2019) and gains values of $K_P = 0.012$, $K_i = 6$ and $K_d = 0.000006$.

On the dc side, the control variable is dc voltage, which controls the active power. The droop strategies are used to hybrid the DC and AC microgrids. Therefore, the droop equation is given as,

$$V = V_{\max} - (K_{dc} \times P_{dc}) \tag{18}$$

Here, V, $V_{\max}$, K_{dc} and P_{dc} are represent the dc link voltage, no load dc link voltage, droop gain, and converter output power, respectively. So that the droop slopes load sharing is proportional to the converters rated power.

$$K_{dc} = \frac{V_{\max} - V_{\min}}{P_{dc,n}} \tag{19}$$

The minimum allowable dc voltage is denoted as $V_{\min}$ and converter rated power is $P_{dc,n}$. Higher droop gains are utilized to enhance the accuracy. However, the microgrid voltage drop is increased. So to control the power sharing, the frequency based approach is employed between the converters.

3.5. AC sub-grid

The AC wind sub system consists of the windmill, wind turbine generator, rectifier, and DC–DC converter. The ac power is generated from the wind turbine, which is controlled through the ANFIS controller. In the ac microgrid, the power supply is associated with the ac bus through the DC–AC converter. The ANFIS has input, output, and membership functions, and it has five layers. Two inputs are in the fuzzy interference framework one is active, and another one is reactive (P and Q), and two outputs, one is the frequency, and another one is voltage (F and V). If the rule-based contains two fuzzy (if–then) rules as follows (Eyghami et al., 2017):

$$\text{If } P \text{ is } A_1 \text{ and } Q \text{ is } B_1, \text{ then } f_1 = p_1 P + q_1 Q + r_1$$
$$\text{If } P \text{ is } A_2 \text{ and } Q \text{ is } B_2, \text{ then } f_2 = p_2 P + q_2 Q + r_2 \tag{20}$$

The ANFIS-based controller might be utilized to ensuring about model authenticity. For the ANFIS controller, the training data association is assembled. The training data under horrendous changes of reactive and active weights are considered to get an accurate model. After getting the training dataset, the ANFIS structure is to be completed. The membership function of input and output are considered in a sort of Gaussian and linear functions. For interlinking of ac and dc, the ac droop control theory is employed. The inverter reference frequency is expressed in Eq. (21),

$$f_{ac} = f_{\max} - (K_{ac}P_{ac}) \tag{21}$$

where reference frequency, no load condition maximum frequency, inverter output power, and droop gain slope are denoted

as f_{ac}, f_{max}, P_{ac} and K_{ac} respectively. So load sharing between the inverters of the droop slope is defined in Eq. (22).

$$K_{ac} = \frac{f_{max} - f_{min}}{P_{ac,n}} \qquad (22)$$

Here, minimum allowable frequency is indicated as f_{min} and inverter rated power is $P_{ac,n}$.

3.6. Interlinking converter

In the hybrid microgrid, there are multiple ac and dc subgrids with different rated dc voltages and rated ac frequencies. A hybrid microgrid contains one dc voltage and one ac voltage; the application scope is limited. The multiple rated dc voltages and ac frequencies are compatible with a proposed hybrid microgrid. The ac subgrids consist of ac DGs in a hybrid microgrid that transforms RES into ac electrical energy. Power sharing will be done inside the subgrids by the particular DCS for the AC subgrid and DC subgrid. However, we have to interface both subgrids together in a controlled way. Subsequently, the interlinking converter is utilized to interface the two sorts of subgrids together. The droop control method for interlinking converters is produced. Here the utilization of the interlinking converter is distinctive, i.e., the flow of power from DC to AC subgrid. The information consolidated is nothing added than abundance generation limits of both subgrids, detected by estimating the dc terminal voltage $V_{1,N}$ and AC frequency f on the two parts of the interlinking converter,

$$f_{pu} = (f - 0.5(f_{max\,imum} + f_{min\,imum}))/(0.5(f_{max\,imum} - f_{min\,imum})) \qquad (23)$$

$$V_{I,N,pu} = \frac{\left(V_{I,N} - 0.5\left(V_{I,N\,max\,imum} + V_{I,N\,min\,imum}\right)\right)}{\left(0.5\left(V_{I,N\,max\,imum} - V_{I,N\,min\,imum}\right)\right)} \qquad (24)$$

where dc terminal voltage of interlinking converter is represented as $V_{I,N}$. From the interlinking converter (IC), the demand power P_d is transferred into ac to the dc grid.

$$P_d = K_{IC}(V_{I,N,pu} - f_{pu}) \qquad (25)$$

While the ac side is normalized, power is equal to the ac side as $V_{I,N,pu} = f_{pu}$, therefore $P_d = 0$. If dc/ac load increases, $V_{I,N,pu}/f_{pu}$ will be decreased. So based on Eq. (25), the power is transferred from dc/ac to the ac/dc sub-grid. The frequency-droop strategy controls the IC, so the dc voltage with frequency is proportional to the output power.

$$f_{dc} = f_{max\,imum} - K_{dc}P_{dc} \qquad (26)$$

This does not affect the dc system components, and the new control parameter is f_{dc} coordinated with IC droop characteristics. The IC is autonomously operated using Eqs. (27) and (28).

$$P_d = K_{IC}(f_{dc,pu} - f_{pu}) \qquad (27)$$

$$f_{dc,pu} = \frac{f_{dc} - 0.5(f_{max\,imum} + f_{min\,imum})}{0.5(f_{max} - f_{min})} \qquad (28)$$

Here, f_{dc} is dc side frequency and minimum and maximum frequency already considered ac frequency.

3.7. Cost reduction by elephant herding optimization

Generation cost is calculating the cost that is used to generate the power for each RES; along with that, we also estimate the maintenance cost, fuel cost, and emission cost for individual energy sources (Elhosseini et al., 2019). The advantage of EHO is that it is easy and very fast because it has no complicated operations. The flow of EHO based optimized cost is given in Fig. 3.
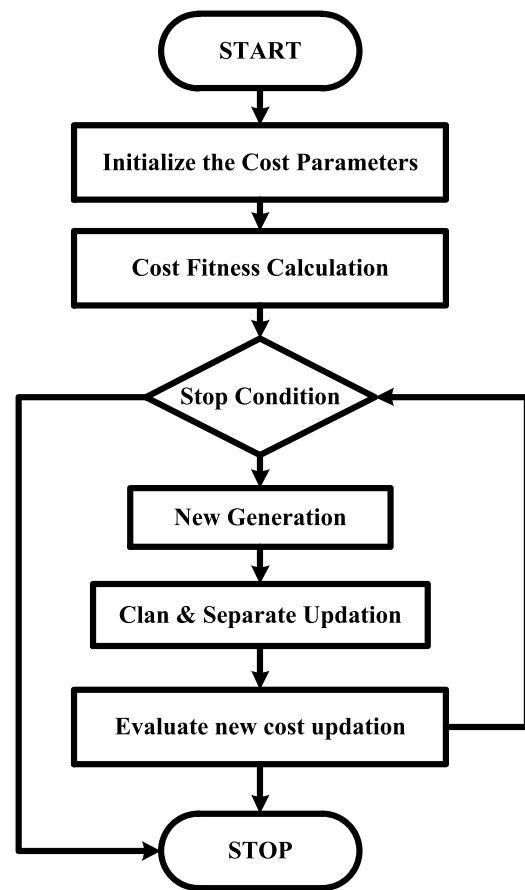

Fig. 3. EHO based optimized cost.

These cost minimization processes can be done by using Elephant herding optimization.

$$C_{G,i}(G_i) = C_{G,m,i}(G_i) + C_{G,e,i}(G_i) \qquad (29)$$

where $C_{G,i}(G_i)$ is the whole active power generation cost of ith generator, $C_{G,e,i}(G_i)$ is represented as the emission penalty for the concerned generator and $C_{G,m,i}(G_i)$ is represented as maintenance cost. The generation cost of the grid is given in Eq. (30),

$$C_{p,i}(P_i) = \alpha_i(P_i^2) + \beta_i(P_i) + \gamma_i \qquad (30)$$

(a) Clan updating operator

The entire population is initially classified into C clans. Every member j of the clan i moves concurring matriarch where matriarch is the elephant k_i with the perfect fitness value in a generation.

$$x_{new,ki,j} = x_{ki,j} + \alpha\left(x_{best,ki} - x_{ki,j}\right) \times R \qquad (31)$$

where $x_{new,ki,j}$ represents modern position of j in clan i and $x_{ki,j}$ is its older position, $x_{best,ki,j}$ is the finest solution of clan k_i, $\alpha \in [0, 1]$ is algorithms parameter. Which resolves the consequence of matriarch and $R \in [0, 1]$ is an arbitrary number worn to develop the diversity of the population in the next steps of the algorithm.

The best position in the clan $x_{best,ki}$ is modernized by the upcoming equation,

$$x_{best,ki} = x_{ki,j} + \beta \times x_{center,ki} \qquad (32)$$

where $\beta \in [0, 1]$ second parameter of the algorithm is which restraints consequences of $x_{center,ki}$ is described as,

$$x_{center,ki,d} = \frac{1}{n} \times \sum_{l=1}^{n_{ki}} x_{ki,l,D} \qquad (33)$$

where $1 \leq D \leq d$ is the dimension and d is the entire dimension of space while n_{ki} is the no. of particles in the clan i.

(b) Separating operator

When solving the issues of optimizations, this separating method can be modeled into a separating operator. According to the below equation, the worst values of the objective function are moved to the next new position.

$$x_{worst,ki} = x_{\min} + (x_{\max} - x_{\min} + 1) \times rand \qquad (34)$$

where $x_{\max}$ and $x_{\min}$ upper and lower bound, parameters $rand \in [0, 1]$ are random number picked from uniform distribution.

3.8. Droop control strategy for cost based hybrid AC–DC load sharing

The power sharing between PV sources is affected by the droop coefficient during DC-bus voltage regulation (Hasan et al., 2016). The conventional droop control is described by,

$$\theta_i = \frac{1}{p}\left(\omega_n - m_{p,i}\ P_{si}\right) \qquad (35)$$

The conventional droop scheme of power sharing completely depends on individual generator reactive and active powers. Although dealing with RES, it does exclude cost as any parameter that is really a significant parameter. The diverse generators can be of different rated capacities in a microgrid system. The cost capacity is converted into per unit depending on their generator abilities to expel this error that is given beneath,

$$C'_{p,i}(P_i) = \frac{C_{P,i}(P_i)}{P_{i,\max}} \qquad (36)$$

where maximum power is denoted as $P_{i,\max}$ that is ith generator can generate.

The generator cost function is the most important consideration that likewise incorporates the no load operation cost. The running cost is required for load sharing purposes. The below alteration is connected to the cost function to exclude the no load cost from the cost function.

$$C''_{P,i}(P_i) = C'_{pi}(P_i) - C'_{p,i}(P_i = 0) \qquad (37)$$

Droop coefficient for active and reactive power is achieved as below,

$$m_{p,i,c} = \frac{\omega_n - \omega_{n,\min}}{C''_{P,\max}} \qquad (38)$$

where, $n_{q,i,c}$ and $m_{p,i,c}$ are reactive and active power droop coefficient with cost, $W_{n,\min}$ are minimum values while operating with droop control.

4. Result and discussion

The entire work is implemented by using the MATLAB tool. The performance of solar energy, wind turbine, and cost minimization is taken out and examined to display the efficiency of the proposed system. The module of PV is Kyocera KC200GT, and the maximum voltage is 26.3 V. Simulation parameters used in this work are given in Table 1.
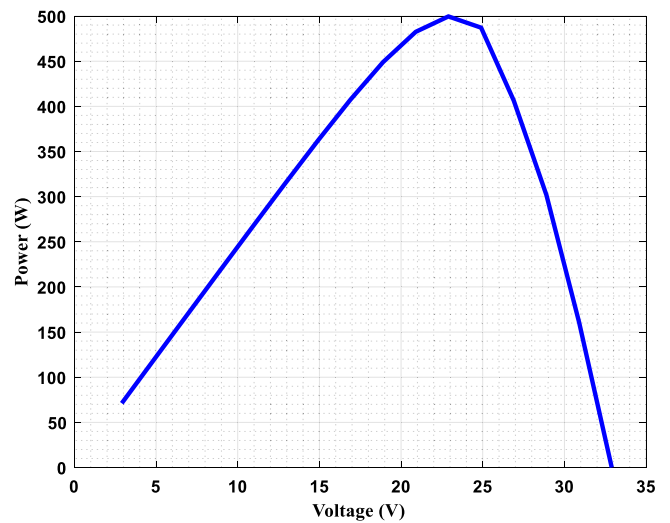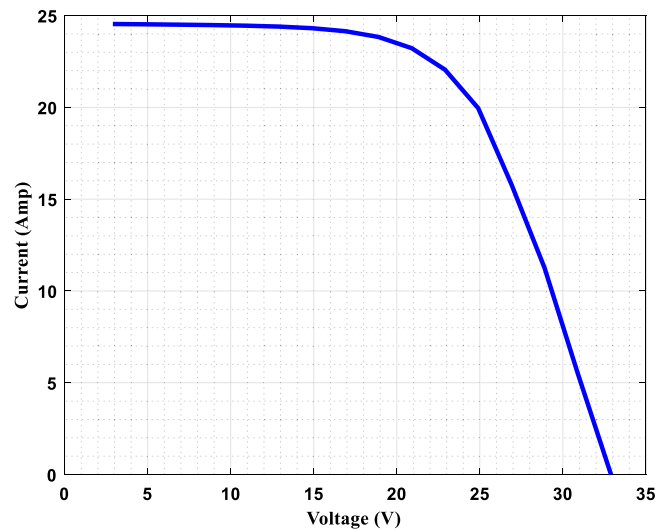

Fig. 4. Voltage vs. power.

Fig. 5. Voltage vs. power.

4.1. PV1 for rating 500 W

(a) Voltage vs. power

The presentation of the voltage vs. power graph is displayed in Fig. 4. Here, by varying voltage, the power is increased. 500 W power is achieved in PV1. At the range of 23 V, the 500 W power is produced.

(b) Voltage vs. current

The performance of the voltage vs. current graph is shown in Fig. 5. Here, by varying voltage, the current is decreased. The current is decreased, when the range of voltage is increased.

4.2. Wind 1 for ratting 300 W

The wind power is shown in Fig. 6 at the rating of 300 W. here, by varying voltage, the power will increase and then slightly decrease. When the range pf voltage reaches 11 V, the wind power will reach the maximum power of 300 W.

Table 1

Simulation parameters.

Parameters	Values	Parameters	Values
Boltzmann constant	1.38e−23	Rotor speed	397 rpm
Short circuit current	8.21 A	Radius	1
Open circuit voltage	32.9 V	Pitch angle	4
Temperature voltage constant	−0.123	Wind speed	10 m/s
Temperature current constant	0.0032	Power rating	300 W
No. of series connected cells	54	Battery rating	34 V, 7 A
Irradiance	1000 W/m^2	Scale & scale factor c & k	2.36 & 1.5
Ideality constant	2	ω_n	314 rad/s
Series resistance	0.1 Ω	V	120 V
Parallel resistance	415.4 Ω	Coefficient s of wind α, β & γ	4.75×10^{-5}, 7.7×10^{-3} & 0.06
PV power rating	500 W	Coefficients of PV	6.2×10^{-5}, 8.69×10^{-3} & 0.08
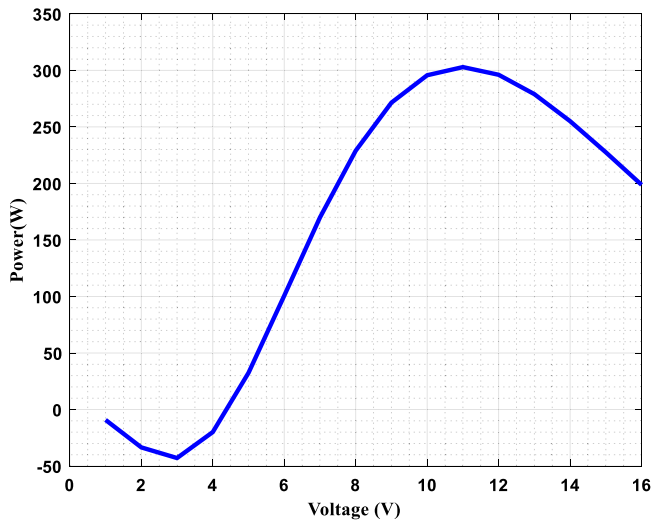
Fig. 6. Wind power at rating 300 W.
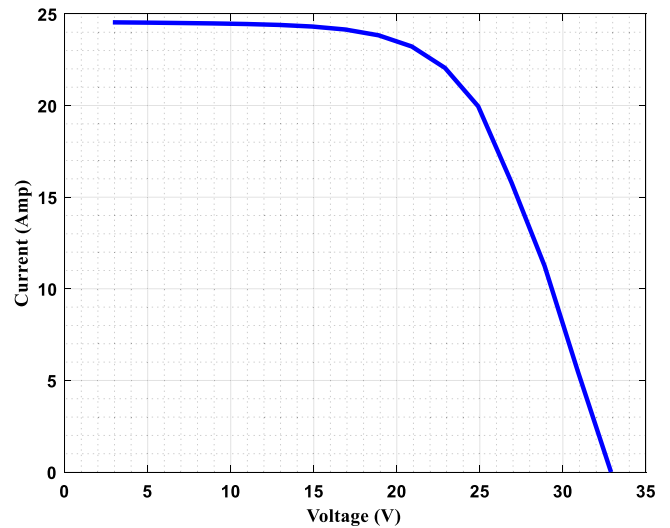

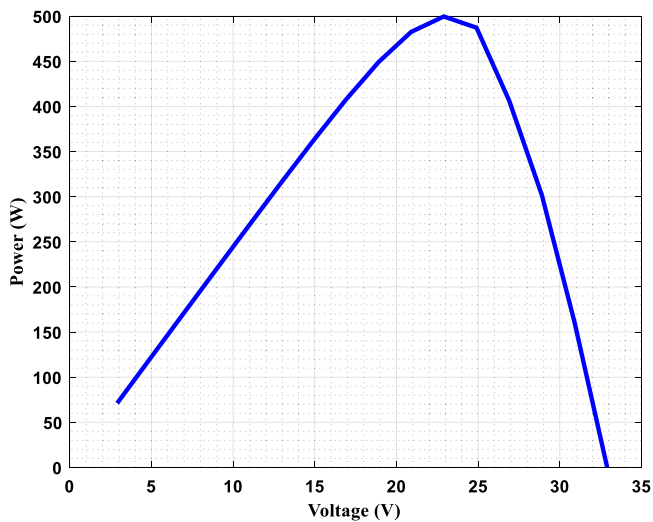**Fig. 8.** Voltage vs. current.

Fig. 7. Voltage vs. power.

4.3. PV2 for rating 500 W

(a) Voltage vs. power

The presentation of the voltage vs. power graph is displayed in Fig. 7. Here, by varying voltage, the power is increased. 500 W power is achieved in PV2. At the range of 23 V, the 500 W power is produced.

(b) Voltage vs. current

The performance of the voltage vs. current graph is shown in Fig. 8. Here, by varying voltage, the current is decreased. The current is decreased, when the range of voltage is increased.

4.4. Wind 2 for ratting 300 W

The wind power is shown in Fig. 9 at the rating of 300 W. Here, by varying voltage, the power will increase and then slightly decrease. When the range pf voltage reaches 11 V, the wind power will reach the maximum power of 300 W.

4.5. Power demand

Fig. 10 shows the load demand for DC power generation. In the hour of 11, the load demand of DC power generation is very high when compared to the other time of hours. At the time of hour 3, the load demand for DC power generation is very low.

Fig. 10 also shows the load demand for AC power generation. In the hour of 4, the load demand of AC power generation is very high when compared to the other hours. In hour 10, the load demand is medium, and at the time of hour 8, the load demand of AC power generation is very low.

4.6. DC link voltage

Fig. 11 shows the comparison of DC link voltage. By the varying time, the DC link voltage will be increased for the rating of 500 W. At the time of above 0.1 s, it will go constant DC link voltage.
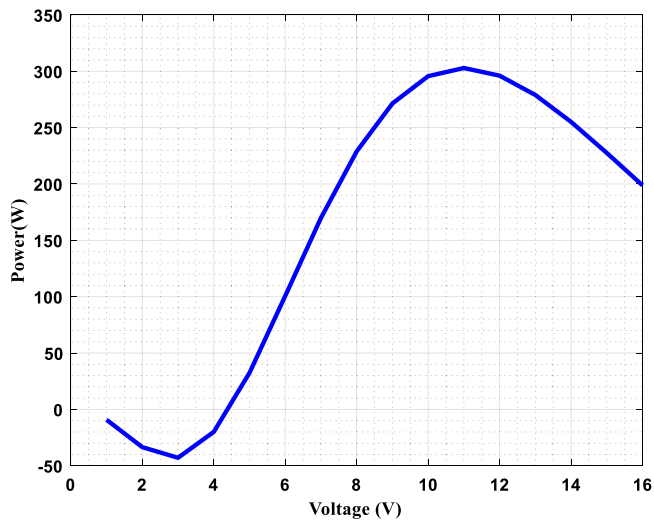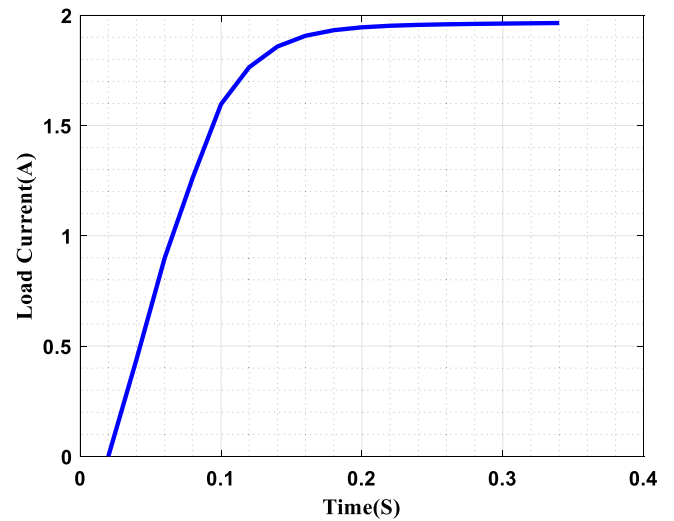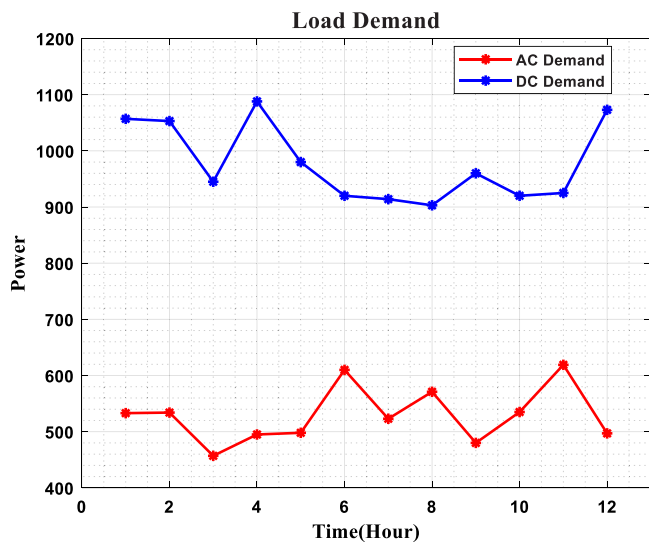
Fig. 9. Voltage vs. current.

Fig. 10. AC–DC power generation.

Fig. 11. DC link voltage.

Fig. 12. Load current.
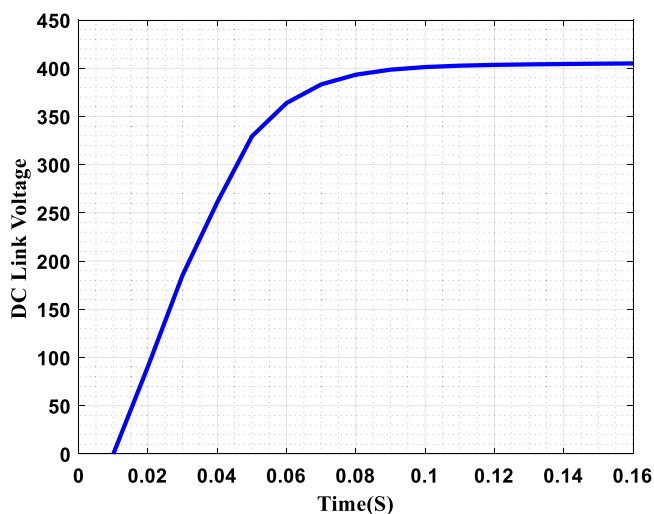
Table 2
Power generation.

Power generated from PV1 (DC)	Power generated from PV2 (DC)	Power generated from Wind1 (AC)	Power generated from Wind2 (AC)
480	485	280	289
460	490	265	280
483	495	275	290
490	485	278	284
475	479	281	276
487	480	263	279
463	485	283	287
496	499	297	289
489	494	269	278
492	496	289	295

4.7. Load current

Fig. 12 display the comparison of load current. By the varying time, the load current will be increased. At the time of above 0.2 s, it will go constant load current.

In our work, the generated power from PV and wind are tabulated in Table 2. Based on the load demand of ac and dc, the load is shared through the interlinking converter. If the ac demand is higher than the generated ac power, the dc power (PV1 and PV2) is shared through the IC. Similarly, if the dc demand is higher than the generated dc power, the ac power (W1 and W2) is shared among the IC. This tactic converts a small ac voltage signal into a dc voltage, where ac signal frequency is relative to the corresponding output power. Hence, dc and ac droop characteristics are coordinated with IC. By using the proposed control method, the load sharing accuracy on ac and dc sources can be enhanced.

Cost based Droop Parameter Estimation

The EHO algorithm is utilized to optimize the cost function in the proposed approach. By varying the function of evaluation, the droop parameter estimation cost will be decreased. The cost is minimized in constant value at the time function evaluation of 20 to 60. The proposed work performance is compared without and with cost based droop parameters. Our proposed work gives better results. The running cost is calculated from the generation cost. The running cost of PV1, PV2, W1, and W2 is 0.4017, 0.4033, 0.2211, and 0.2010, respectively. This running cost is determined based on the condition of ac and dc load sharing. If the load is changed, the cost range also will be changed, and then the optimization algorithm of EPO is utilized to optimize the cost

Table 3
Droop coefficients of ac and dc.

Droop coefficient	Values
$k_{ac,1}$	0.002356
$k_{ac,2}$	0.002413
$k_{dc,1}$	0.004032
$k_{dc,2}$	0.004008

function. Hence, the cost based load sharing droop coefficient parameter is achieved. The droop coefficient ($m_{p,i}$) of PV1, PV2, W1, and W2 is 8.71, 8.67, 15.82 and 17.40, respectively. The cost based droop coefficient parameter is inversely proportional to the load sharing based cost value. PV power sharing ratio is 1.004, which equals to cost coefficients ratio PV1 and PV2. Then the wind power sharing ratio is 0.909, which equals to cost coefficients ratio of W1 and W2. Therefore, these results confirm that the cost-based droop controller assists power sharing in the ratio of cost functions.

Without cost based droop parameter estimation

For the dc and ac droop characteristics, the load sharing between the dc and ac microgrids is considered without cost-based droop control strategy for comparison purposes. The load sharing amongst the inverter droop coefficient k_{ac} is performed on the wind sources. The load sharing amongst the converter droop coefficient k_{dc} is performed on the PV sources, which are given in Table 3.

The normalized dc voltage and normalized ac frequency are determined for the normalized droop approach. The normalized frequency $f_{ac,1}$ & $f_{ac,2}$ is 0.9461 and 0.9172, respectively. Then the normalized voltage of $V_{I,Npu1}$ & $V_{I,Npu2}$ is 4.668 and 4.679, respectively. The presented interlinking droop strategy accurately shares the dc and ac loads between dc and ac sources connected with the interlinking converter to the common bus. The load sharing ratio is proportional to the droop coefficients. Load sharing of coefficient of PV1, PV2, W1, and W2 is 0.00201, 0.002004, 0.00336, and 0.00344, respectively. If the ac or dc load increases, $f_{ac,pu}$ or $V_{I,Npu}$ decreases, the dc or ac power is transferred into the dc or ac grid. Then the IC power is transferred from ac to dc grid while the same as dc power is transferred into ac grid. The interlinking topology coordinated with the interlinking droop characteristics. For $K_{ic} = 1000$, the dc load and ac load 3722 watts and 3762 watts which is satisfied the load demand. For better load sharing performance, the ratio of the droop coefficient is equal to the ratio of load sharing between the RES. The ac droop coefficient ratio of 0.97 is equal to the ratio of load sharing between ac sources. The dc droop coefficient ratio 1.006 equals the load sharing ratio between dc sources. Based on this ratio, the power sharing is perfectly done between ac and dc grids.

Fig. 13 shows the performance of cost by comparing some existing techniques like GA and PSO (Bansal et al., 2013). The total cost is calculated by varying the number of iterations. At the 20th iteration, the cost of the existing GA is 0.5, PSO is 0.8, and the cost of the proposed EHO method is 0.3. The proposed EHO achieve less cost with less number of iteration when compared to the existing approaches. From the total cost comparison graph, we clearly know the proposed approach's effectiveness. Table 4 shows the advantages and disadvantages of the proposed and previous methods to show the proposed method's effectiveness.

5. Experimental setup

The controller hardware-in-the-loop (CHIL) experiments were executed in the OPAL-RT real time simulation system to verify the effectiveness of the proposed uniform control strategy. In this CHIL experiment, the uniform control strategy was implemented
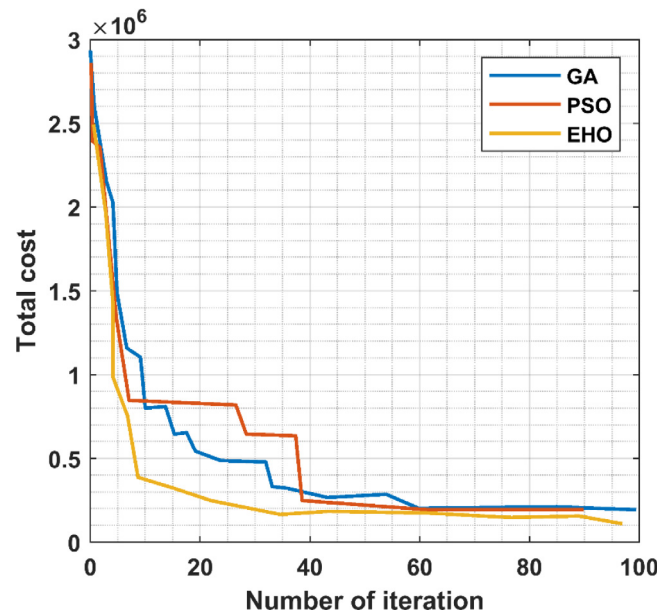

Fig. 13. Total cost comparison.

Table 4
Advantage and Disadvantages of proposed method and previous method.

Methods	Advantages	Disadvantages
GA	Easy to implement	Time consuming
PSO	Efficient global search algorithm	Slow convergence
Proposed EHO	Fast Convergence	Computation is large

in a DSP (TMS320F28335) for the bidirectional ac/dc interlinking converter, although in the OPAL-RT real time simulator, the other system element were simulated as given in Fig. 14. In this experiment, the ac and dc loads are set as pure resistive loads.

Figure shows the experimental graph of the current and voltage of PV by varying times. The range to set the current is 4 A, and voltage is 9 V by changing time 8 s for the calculation of the experimental waveform and the correspoding waveforms are shown in Fig. 15.

Fig. 16 shows the experimental performance of the bidirectional ac/dc interlinking converter in power dispatch mode. At first, using the droop control strategy, the ac/dc bus voltage was regulated around the nominal values. At this moment, the communication network was not available and the bidirectional ac/dc interlinking converter was in power dispatch mode with GPS operation from ac to dc subgrid by transferring 2.2 kW. The bidirectional ac/dc interlinking converter power flow was subsequently changed from 2.2 kW to −2 kW. The effectiveness of power dispatch mode under uniform control has been verified.

Fig. 17 demonstrates the mode transfer from power dispatch to Dc voltage regulation for a uniform controlled bidirectional ac/dc interlinking converter. DC voltage and AC frequency were maintained within the tolerance band after the load steps down. By transferring the right amount of active power to DC load, the bidirectional ac/dc interlinking converter under able to maintain stable DC-voltage regulation operation. Due to the lighter load, the slight increment of both ac frequency and dc voltage was on the DC side.

Fig. 18 demonstrates the mode transfer from power dispatch to Dc voltage regulation for a uniform controlled bidirectional ac/dc interlinking converter. The amplitude and frequency of the ac voltage were smoothly maintained around the nominal values if the MVS failed and was abruptly disconnected from the ac
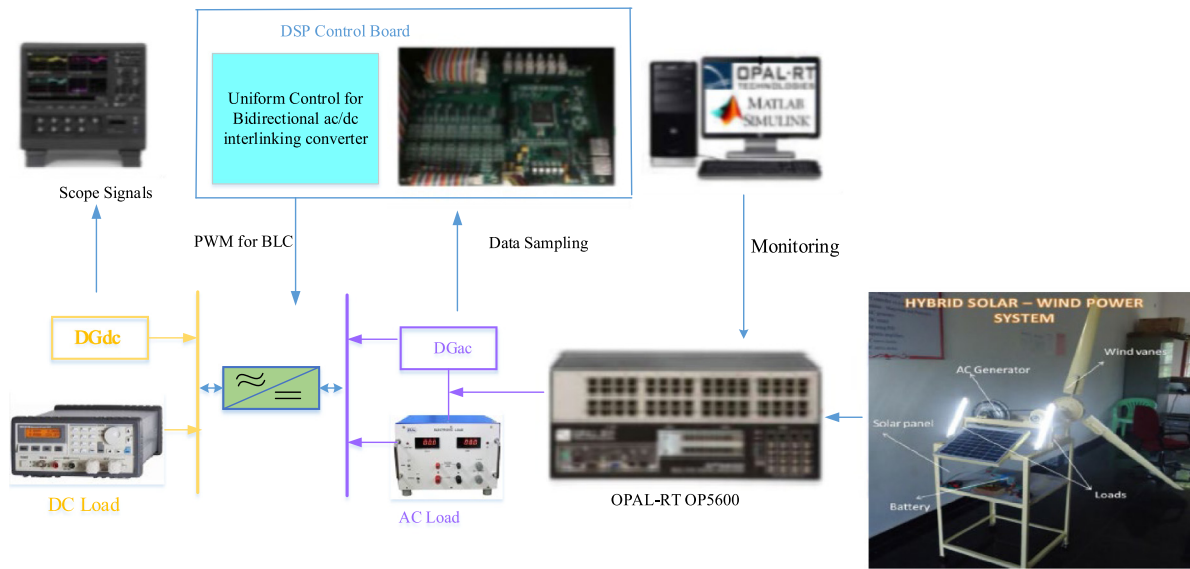
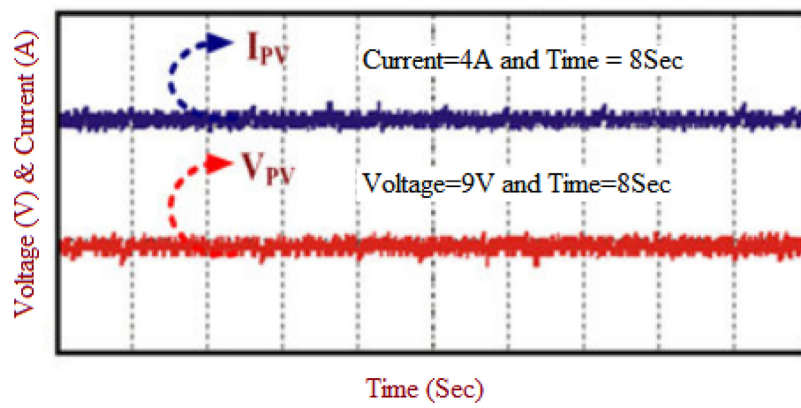**Fig. 14.** Experimental setup of proposed design.

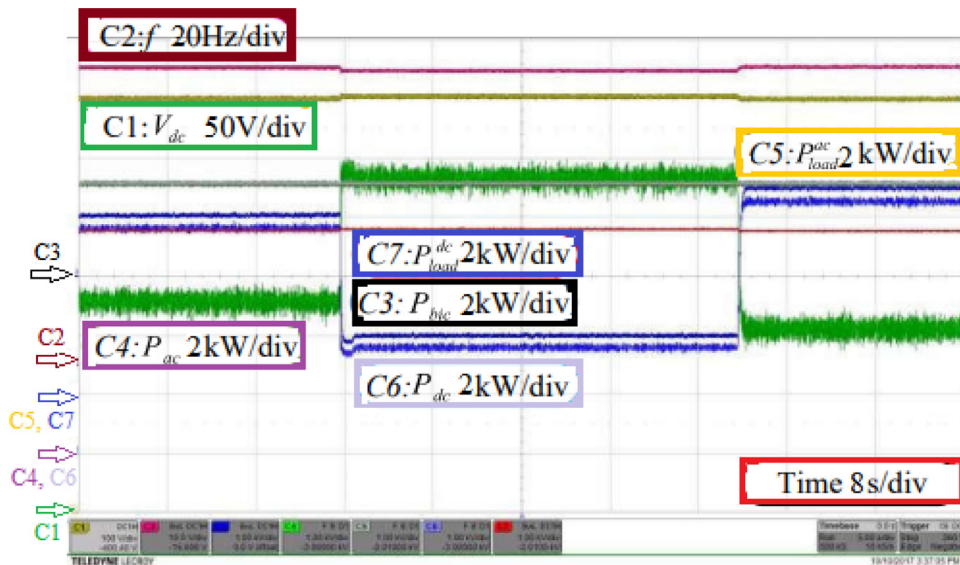**Fig. 15.** Experimental waveform of I_{PV} and V_{PV}.

Fig. 16. Experimental waveform of bidirectional ac/dc interlinking converter in power dispatch mode with load change.
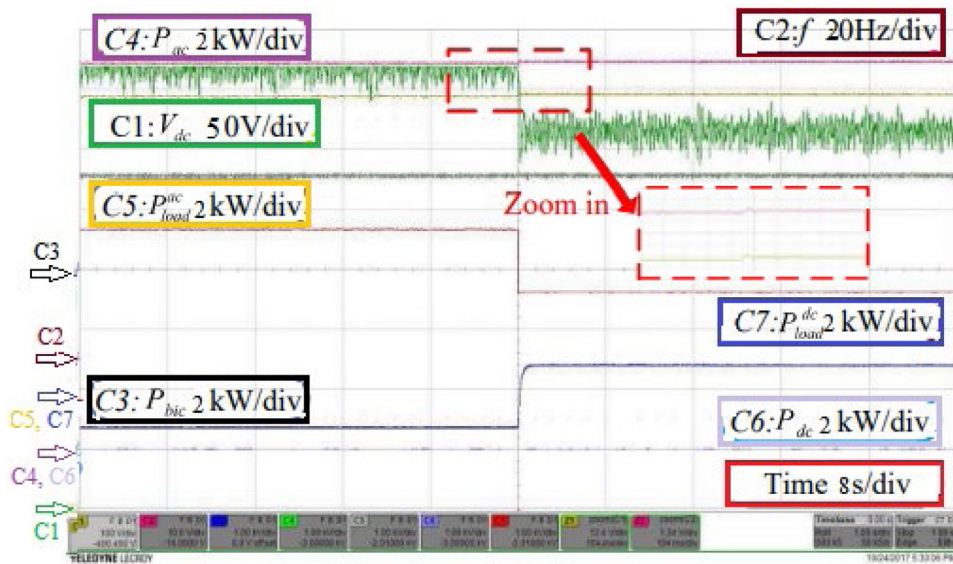
Fig. 17. Experimental waveform of power profile and ac frequency/dc voltage for DC voltage regulation.
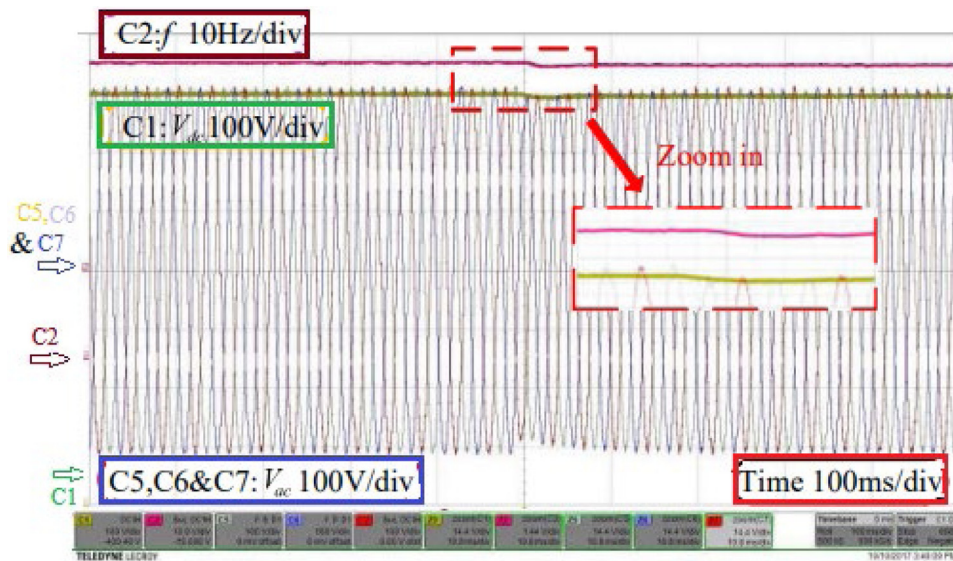

Fig. 18. Experimental waveform of DC voltage and AC voltage/frequency from power dispatch to AC-voltage regulation.

bus at t = 0.6 s The effectiveness of the uniform controlled bidirectional ac/dc interlinking converter from power dispatch to AC-voltage regulation mode has been verified.

6. Conclusion

This paper displays the energy management method of a hybrid system like PV, a wind turbine with a storage battery has been developed. It also tends to ideal operation and energy management of hybrid AC–DC microgrid utilizing a speculative system. To create the microgrid, the interlinking converter is utilized. In our paper, two PV, two wind and two batteries are utilized. From that, the uncertainty of PV irradiance and wind speed has been modeled. The droop control strategies are utilized in the AC and DC microgrid. It is observed that AC and DC sections of the microgrid have excellent cooperation in power exchange and energy to mitigate the total expense of the hybrid microgrid. Also, by using the Elephant Herding Optimization (EHO) algorithm, the cost price has been mitigated. The EPO based cost minimized

load sharing and without cost based load sharing, performance was also investigated. The entire process is implemented under the MATLAB platform, and the performances are taken in terms of power demand, DC link voltage, power, current, and voltage for wind and solar. The total cost was compared by using some existing techniques like GA and PSO with the proposed technique, and the cost of the proposed is 0.3 (i.e., very low) than the existing techniques. In the future, we will provide experimental validation in order to validate the simulation result for the power management system. By these validations, the performance of this work can be enhanced further in the future.

CRediT authorship contribution statement

T. Narasimha Prasad: Investigation, Development, Writing – review & editing. **S. Devakirubakaran:** Investigation, Conceptualization, Writing - review & editing. **S. Muthubalaji:** Investigation, Formal analysis, Writing – review & editing. **S. Srinivasan:** Investigation, Formal analysis, Writing – review & editing.

Karthikeyan B.: Conceptualization, Formal analysis, Writing – review & editing. **Palanisamy R.:** Conceptualization, Writing – review & editing. **Mohit Bajaj:** Writing – review & editing, Supervision. **Hossam M. Zawbaa:** Funding, Writing – review & editing. **Salah Kamel:** Supervision, Writing – review & editing.

Declaration of competing interest

The authors declare that they have no known competing financial interests or personal relationships that could have appeared to influence the work reported in this paper.

Data availability

Data will be made available on request.

Acknowledgments

References

Aljafari, B., Samithas, D., Balachandran, P.K., Anandan, S., Babu, T.S., 2022. Performance analysis of PLA material based micro-turbines for low wind speed applications. Polymers 14 (19), 4180. http://dx.doi.org/10.3390/polym14194180.

Allaoua, B., Asnoune, K., Mebarki, B., 2017. Energy management of PEM fuel cell/supercapacitor hybrid power sources for an electric vehicle. Int. J. Hydrogen Energy 42 (33), 21158–21166.

Alsiraji, H.A., El-Shatshat, R., 2021. Virtual synchronous machine/dual-droop controller for parallel interlinking converters in hybrid AC–DC microgrids. Arab. J. Sci. Eng. 46 (2), 983–1000.

Armghan, H., Yang, M., Armghan, A., Ali, N., Wang, M.Q., Ahmad, I., 2020. Design of integral terminal sliding mode controller for the hybrid AC/DC microgrids involving renewables and energy storage systems. Int. J. Electr. Power Energy Syst. 119, 105857.

Bansal, A.K., Kumar, R., Gupta, R.A., 2013. Economic analysis and power management of a small autonomous hybrid power system (SAHPS) using biogeography based optimization (BBO) algorithm. IEEE Trans. Smart Grid 4 (1), 638–648.

Cherukuri, S.K., et al., 2021. Power enhancement in partial shaded photovoltaic system using spiral pattern array configuration scheme. IEEE Access 9, 123103–123116. http://dx.doi.org/10.1109/ACCESS.2021.3109248.

Dewangan, D., Mudliar, A., Deb, S., Banik, A., Bhusnur, S., 2021. Fuzzy logic control for energy management in distributed generation paradigm. In: 2021 International Conference on Advances in Electrical, Computing, Communication and Sustainable Technologies. ICAECT, IEEE, pp. 1–5.

Ding, L., Deng, W., Pei, W., Zhuang, Y., 2022. Dynamic performance analysis of low-voltage AC/DC hybrid power distribution system under multiple uncertainties. Energy Rep. 8, 948–956. http://dx.doi.org/10.1016/j.egyr.2022.08.136.

Elhosseini, M.A., El Sehiemy, R.A., Rashwan, Y.I., Gao, X.Z., 2019. On the performance improvement of elephant herding optimization algorithm. Knowl.-Based Syst. 166, 58–70.

Esfahani, M.S.G., Savaghebi, M., 2021. A decentralized control strategy based on VI droop for enhancing dynamics of autonomous hybrid AC/DC microgrids. IEEE Trans. Power Electron..

Espina, E., Cardenas-Dobson, R., Simpson-Porco, J.W., Saez, D., Kazerani, M., 2020. A consensus-based secondary control strategy for hybrid ac/dc microgrids with experimental validation. IEEE Trans. Power Electron..

Eyghami, S., Mokhtari, H., Blaabjerg, F., 2017. Autonomous operation of a hybrid AC/DC microgrid with multiple interlinking converters. IEEE Trans. Smart Grid 9 (6), 6480–6488.

Faisal, M., Hannan, M.A., Ker, P.J., Rahman, M.A., Begum, R.A., Mahlia, T.M.I., 2020. Particle swarm optimised fuzzy controller for charging–discharging and scheduling of battery energy storage system in MG applications. Energy Rep. 6, 215–228.

Farhat, O., Khaled, M., Faraj, J., Hachem, F., Taher, R., Castelain, C., 2022. A short recent review on hybrid energy systems: Critical analysis and recommendations. Energy Rep. 8, 792–802. http://dx.doi.org/10.1016/j.egyr.2022.07.091.

Fu, Z., Zhu, L., Tao, F., Si, P., Sun, L., 2020. Optimization based energy management strategy for fuel cell/battery/ultracapacitor hybrid vehicle considering fuel economy and fuel cell lifespan. Int. J. Hydrogen Energy 45 (15), 8875–8886.

Grisales-Noreña, L.F., Montoya, O.D., Ramos-Paja, C.A., 2020. An energy management system for optimal operation of BSS in DC distributed generation environments based on a parallel PSO algorithm. J. Energy Storage 29, 101488.

Gupta, S., Garg, R., Singh, A., 2020. ANFIS-based control of multi-objective grid connected inverter and energy management. J. Inst. Eng. (India): Ser. B 101 (1), 1–14.

Han, Y., Yang, H., Li, Q., Chen, W., Zare, F., Guerrero, J.M., 2020. Mode-triggered droop method for the decentralized energy management of an islanded hybrid PV/hydrogen/battery DC microgrid. Energy 199, 117441.

Hannan, M.A., Tan, S.Y., Al-Shetwi, A.Q., Jern, K.P., Begum, R.A., 2020. Optimized controller for renewable energy sources integration into microgrid: Functions, constraints and suggestions. J. Clean. Prod. 256, 120419.

Hasan, M.A., Vemula, N.K, Parida, S.K., 2016. Cost based dynamic load dispatch for an autonomous parallel converter hybrid AC-DC microgrid. In: 2016 National Power Systems Conference. NPSC, IEEE, pp. 1–5.

Hesaroor, K., Das, D., 2020. Improved modified Newton raphson load flow method for islanded microgrids. In: 2020 IEEE 17th India Council International Conference. INDICON, IEEE, pp. 1–6.

Islam, M.H., Hossain, M.S., Tara, K., Khan, M.A.G., Kundu, P.C, 2020. Droop based dynamic load sharing approach for islanded microgrid. In: 2020 International Conference on Emerging Smart Computing and Informatics. ESCI, IEEE, pp. 170–174.

Jafari, A., Ganjehlou, H.G., Khalili, T., Bidram, A., 2020. A fair electricity market strategy for energy management and reliability enhancement of islanded multi-microgrids. Appl. Energy 270, 115170.

Kumar, D., Mathur, H.D., Bhanot, S., Bansal, R.C., 2020. Modeling and frequency control of community micro-grids under stochastic solar and wind sources. Eng. Sci. Technol. Int. J. 23 (5), 1084–1099.

Lv, Z., Zhang, Y., Yu, M., Xia, Y., Wei, W., 2020. Decentralised coordinated energy management for hybrid AC/DC microgrid by using fuzzy control strategy. IET Renew. Power Gener. 14 (14), 2649–2656.

Manyonge, A.W., Ochieng, R.M., Onyango, F.N., Shichikha, J.M., 2012. Mathematical modelling of wind turbine in a wind energy conversion system: Power coefficient analysis. Appl. Math. Sci. 6 (91), 4527–4536.

Mayer, M.J., Szilágyi, A., Gróf, G., 2020. Environmental and economic multi-objective optimization of a household level hybrid renewable energy system by genetic algorithm. Appl. Energy 269, 115058.

Mousazadeh Mousavi, S.Y., Jalilian, A., Savaghebi, M., Guerrero, J.M., 2018. Power quality enhancement and power management of a multi-functional interfacing inverter for PV and battery energy storage system. Int. Trans. Electr. Energy Syst. 28 (12), e2643.

Naderi, Y., Hosseini, S.H., Ghassemzadeh, S., Mohammadi-Ivatloo, B., Savaghebi, M., Vasquez, J.C., Guerrero, J.M., 2020. Power quality issues of smart microgrids: applied techniques and decision making analysis. In: Decision Making Applications in Modern Power Systems. Academic Press, pp. 89–119.

Naidu, R.P.K., Meikandasivam, S., 2020. Power quality enhancement in a grid-connected hybrid system with coordinated PQ theory & fractional order PID controller in DPFC. Sustain. Energy Grids Netw. 21, 100317.

Narang, D., Ingram, M., Li, X., Stout, S., Hotchkiss, E., Bhat, A., Murthy, S., Keen, J., Shah, C., Baggu, M., Latif, A., 2021. Considerations for Distributed Energy Resource Integration in Puerto Rico: DOE Multi-Lab Grid Modeling Support for Puerto Rico. Analytical Support for Interconnection and IEEE Std 1547-2018 National Renewable Energy Laboratory (Task 3.0) (No. NREL/TP-5D00-77127), National Renewable Energy Lab.(NREL), Golden, CO (United States).

Nayak, B., Mohapatra, A., Mohanty, K.B., 2019. Parameter estimation of single diode PV module based on GWO algorithm. Renew. Energy Focus 30, 1–12.

Oruganti, V.S.R.V., Dhanikonda, V.S.S.S., Mortezaei, A., Busarello, T.D.C., Simões, M.G., 2020. Power management algorithm for a conservative power theory battery storage based multi-functional three phase grid connected PV inverter. Int. Trans. Electr. Energy Syst. 30 (11), e12605.

Peña-Aguirre, J.C., Barranco-Gutiérrez, A.I., Padilla-Medina, J.A., Espinosa-Calderon, A., Pérez-Pinal, F.J., 2020. Fuzzy logic power management strategy for a residential DC-microgrid. IEEE Access 8, 116733–116743.

Qin, H., Xie, S., Xun, Q., Zhang, F., Xu, Z., Wang, L., 2022. An optimized parameter design method of SiC/Si hybrid switch considering turn-off current spike. Energy Rep. 8, 789–797. http://dx.doi.org/10.1016/j.egyr.2022.08.029.

Reyes, E.D., Bretas, A.S., Rivera, S., 2020. Marginal uncertainty cost functions for solar photovoltaic, wind energy, hydro generators, and plug-in electric vehicles. Energies 13 (23), 6375.

Roumila, Z., Rekioua, D., Rekioua, T., 2017. Energy management based fuzzy logic controller of hybrid system wind/photovoltaic/diesel with storage battery. Int. J. Hydrogen Energy 42 (30), 19525–19535.

Shravan, R.V.S.E., Vyjayanthi, C., 2020. Active power filtering using interlinking converter in droop controlled islanded hybrid AC-DC microgrid. Int. Trans. Electr. Energy Syst. 30 (5), e12333.

Sridhar, N., Kowsalya, M., 2021. Enhancement of power management in micro grid system using adaptive ALO technique. J. Ambient Intell. Humaniz. Comput. 12 (2), 2163–2182.

Toghani Holari, Y., Taher, S.A., Mehrasa, M., 2020. Distributed energy storage system-based non-linear control strategy for hybrid microgrid power management included wind/PV units in grid-connected operation. Int. Trans. Electr. Energy Syst. 30 (2), e12237.

Wang, C., Zhang, Z., Abedinia, O., Farkoush, S.G., 2021. Modeling and analysis of a microgrid considering the uncertainty in renewable energy resources, energy storage systems and demand management in electrical retail market. J. Energy Storage 33, 102111.

Zeng, W., Zhu, W., Hui, T., Chen, L., Xie, J., Yu, T., 2020. An IMC-pid controller with particle swarm optimization algorithm for MSBR core power control. Nucl. Eng. Des. 360, 110513.

Zhang, Y., Chen, C., Hong, T., Cui, B., Chen, B., Qiu, F., 2020. Robust synthesis of wind turbine generators to support microgrid frequency considering linearization-induced uncertainty. arXiv preprint arXiv:2003.02905.